

Ultrathin, high-efficiency, broad-band, omni-acceptance, organic solar cells enhanced by plasmonic cavity with subwavelength hole array

Stephen Y. Chou* and Wei Ding

NanoStructure Laboratory, Department of Electrical Engineering, Princeton University, Princeton, New Jersey 08544, USA

**chou@princeton.edu*

Abstract: Three of central challenges in solar cells are high light coupling into solar cell, high light trapping and absorption in a sub-absorption-length-thick active layer, and replacement of the indium-tin-oxide (ITO) transparent electrode used in thin-film devices. Here, we report a proposal and the first experimental study and demonstration of a new ultra-thin high-efficiency organic solar cell (SC), termed “plasmonic cavity with subwavelength hole-array (PlaCSH) solar cell”, that offers a solution to all three issues with unprecedented performances. The ultrathin PlaCSH-SC is a thin plasmonic cavity that consists of a 30 nm thick front metal-mesh electrode with subwavelength hole-array (MESH) which replaces ITO, a thin (100 nm thick) back metal electrode, and in-between a polymer photovoltaic active layer (P3HT/PCBM) of 85 nm thick (1/3 average absorption-length). Experimentally, the PlaCSH-SCs have achieved (1) light coupling-efficiency/absorptance as high as 96% (average 90%), broad-band, and Omni acceptance (light coupling nearly independent of both light incident angle and polarization); (2) an external quantum efficiency of 69% for only 27% single-pass active layer absorptance; leading to (3) a 4.4% power conversion efficiency (PCE) at standard-solar-irradiation, which is 52% higher than the reference ITO-SC (identical structure and fabrication to PlaCSH-SC except MESH replaced by ITO), and also is among the highest PCE for the material system that was achievable previously only by using thick active materials and/or optimized polymer compositions and treatments. In harvesting scattered light, the Omni acceptance can increase PCE by additional 81% over ITO-SC, leading to a total 175% increase (i.e. 8% PCE). Furthermore, we found that (a) after formation of PlaCSH the light reflection and absorption by MESH are reduced by 2 to 6 fold from the values when it is alone; and (b) the sheet resistance of a 30 nm thick MESH is 2.2 ohm/sq or less—4.5 fold or more lower than the best reported value for a 100 nm thick ITO film, giving a lowest reflectance-sheet-resistance product. Finally, fabrication of PlaCSH has used nanoimprint on 4” wafer and is scalable to roll-to-roll manufacturing. The designs, fabrications, and findings are applicable to thin solar cells in other materials.

© 2012 Optical Society of America

OCIS codes: (350.6050) Solar energy; (220.4241) Nanostructure fabrication; (250.5403) Plasmonics.

References and links

1. E. Yablonovitch and G. D. Cody, “Intensity enhancement in textured optical sheets for solar-cells,” *IEEE Trans. Electron. Dev.* **29**(2), 300–305 (1982).

2. H. Kiess and W. Rehwald, "On the ultimate efficiency of solar-cells," *Sol. Energy Mater. Sol. Cells* **38**(1-4), 45–55 (1995).
3. A. V. Shah, R. Platz, and H. Keppner, "Thin-film silicon solar-cells—a review and selected trends," *Sol. Energy Mater. Sol. Cells* **38**(1-4), 501–520 (1995).
4. C. Heine and R. H. Morf, "Submicrometer gratings for solar-energy applications," *Appl. Opt.* **34**(14), 2476–2482 (1995).
5. J. Zhao and M. A. Green, "Optimized antireflection coatings for high-efficiency silicon solar-cells," *IEEE Trans. Electron. Dev.* **38**(8), 1925–1934 (1991).
6. J. H. Zhao, A. H. Wang, M. A. Green, and F. Ferrazza, "19.8% efficient "honeycomb" textured multicrystalline and 24.4% monocrystalline silicon solar cells," *Appl. Phys. Lett.* **73**(14), 1991–1993 (1998).
7. E. Yablonovitch, "Statistical ray optics," *J. Opt. Soc. Am.* **72**(7), 899–907 (1982).
8. S. Y. Chou, Y. Liu, and P. B. Fischer, "Terahertz Gaas metal-semiconductor-metal photodetectors with 25 nm finger spacing and finger width," *Appl. Phys. Lett.* **61**(4), 477–479 (1992).
9. M. G. Kang and L. J. Guo, "Nanoimprinted semitransparent metal electrodes and their application in organic light-emitting diodes," *Adv. Mater. (Deerfield Beach Fla.)* **19**(10), 1391–1396 (2007).
10. J. Y. Lee, S. T. Connor, Y. Cui, and P. Peumans, "Solution-processed metal nanowire mesh transparent electrodes," *Nano Lett.* **8**(2), 689–692 (2008).
11. N. P. Sergeant, A. Hadipour, B. Niesen, D. Cheyins, P. Heremans, P. Peumans, and B. P. Rand, "Design of transparent anodes for resonant cavity enhanced light harvesting in organic solar cells," *Adv. Mater. (Deerfield Beach Fla.)* **24**(6), 728–732 (2012).
12. H. R. Stuart and D. G. Hall, "Island size effects in nanoparticle-enhanced photodetectors," *Appl. Phys. Lett.* **73**(26), 3815–3817 (1998).
13. M. Westphalen, U. Kreibig, J. Rostalski, H. Luth, and D. Meissner, "Metal cluster enhanced organic solar cells," *Sol. Energy Mater. Sol. Cells* **61**(1), 97–105 (2000).
14. B. P. Rand, P. Peumans, and S. R. Forrest, "Long-range absorption enhancement in organic tandem thin-film solar cells containing silver nanoclusters," *J. Appl. Phys.* **96**(12), 7519–7526 (2004).
15. H. Mertens, J. Verhoeven, A. Polman, and F. D. Tichelaar, "Infrared surface plasmons in two-dimensional silver nanoparticle arrays in silicon," *Appl. Phys. Lett.* **85**(8), 1317–1319 (2004).
16. D. M. Schaadt, B. Feng, and E. T. Yu, "Enhanced semiconductor optical absorption via surface plasmon excitation in metal nanoparticles," *Appl. Phys. Lett.* **86**(6), 063106 (2005).
17. D. Derkacs, S. H. Lim, P. Matheu, W. Mar, and E. T. Yu, "Improved performance of amorphous silicon solar cells via scattering from surface plasmon polaritons in nearby metallic nanoparticles," *Appl. Phys. Lett.* **89**(9), 093103 (2006).
18. E. P. Kartalov, A. Scherer, S. R. Quake, C. R. Taylor, and W. F. Anderson, "Experimentally validated quantitative linear model for the device physics of elastomeric microfluidic valves," *J. Appl. Phys.* **101**(6), 64505 (2007).
19. R. B. Konda, R. Mundle, H. Mustafa, O. Bamiduro, A. K. Pradhan, U. N. Roy, Y. Cui, and A. Burger, "Surface plasmon excitation via Au nanoparticles in n-CdSe/p-Si heterojunction diodes," *Appl. Phys. Lett.* **91**(19), 191111 (2007).
20. J. K. Mapel, M. Singh, M. A. Baldo, and K. Celebi, "Plasmonic excitation of organic double heterostructure solar cells," *Appl. Phys. Lett.* **90**(12), 121102 (2007).
21. M. Kirkengen, J. Bergli, and Y. M. Galperin, "Direct generation of charge carriers in c-Si solar cells due to embedded nanoparticles," *J. Appl. Phys.* **102**(9), 093713 (2007).
22. K. Tvingstedt, N.-K. Persson, O. Inganäs, A. Rahachou, and I. V. Zozoulenko, "Surface plasmon increase absorption in polymer photovoltaic cells," *Appl. Phys. Lett.* **91**(11), 113514 (2007).
23. C. Hägglund, M. Zach, G. Petersson, and B. Kasemo, "Electromagnetic coupling of light into a silicon solar cell by nanodisk plasmons," *Appl. Phys. Lett.* **92**(5), 053110 (2008).
24. P. Matheu, S. H. Lim, D. Derkacs, C. McPheeters, and E. T. Yu, "Metal and dielectric nanoparticle scattering for improved optical absorption in photovoltaic devices," *Appl. Phys. Lett.* **93**(11), 113108 (2008).
25. K. Nakayama, K. Tanabe, and H. A. Atwater, "Plasmonic nanoparticle enhanced light absorption in GaAs solar cells," *Appl. Phys. Lett.* **93**(12), 121904 (2008).
26. S. S. Kim, S. I. Na, J. Jo, D. Y. Kim, and Y. C. Nah, "Plasmon enhanced performance of organic solar cells using electrodeposited Ag nanoparticles," *Appl. Phys. Lett.* **93**(7), 073307 (2008).
27. A. J. Morfa, K. L. Rowlen, T. H. Reilly III, M. J. Romero, and J. Van De Lagemaat, "Plasmon-enhanced solar energy conversion in organic bulk heterojunction photovoltaics," *Appl. Phys. Lett.* **92**(1), 013504 (2008).
28. N. C. Lindquist, W. A. Luhman, S.-H. Oh, and R. J. Holmes, "Plasmonic nanocavity arrays for enhanced efficiency in organic photovoltaic cells," *Appl. Phys. Lett.* **93**(12), 123308 (2008).
29. C. Hägglund, M. Zach, and B. Kasemo, "Enhanced charge carrier generation in dye sensitized solar cells by nanoparticle plasmons," *Appl. Phys. Lett.* **92**(1), 013113 (2008).
30. F.-J. Haug, T. Söderström, O. Cubero, V. Terrazzoni-Daudrix, and C. Ballif, "Plasmonic absorption in textured silver back reflectors of thin film solar cells," *J. Appl. Phys.* **104**(6), 064509 (2008).
31. R. A. Pala, J. White, E. Barnard, J. Liu, and M. L. Brongersma, "Design of plasmonic thin-film solar cells with broadband absorption enhancements," *Adv. Mater. (Deerfield Beach Fla.)* **21**(34), 3504–3509 (2009).
32. H. A. Atwater and A. Polman, "Plasmonics for improved photovoltaic devices," *Nat. Mater.* **9**(3), 205–213 (2010).

33. N. I. Landy, S. Sajuyigbe, J. J. Mock, D. R. Smith, and W. J. Padilla, "Perfect metamaterial absorber," *Phys. Rev. Lett.* **100**(20), 207402 (2008).
34. J. S. White, G. Veronis, Z. Yu, E. S. Barnard, A. Chandran, S. Fan, and M. L. Brongersma, "Extraordinary optical absorption through subwavelength slits," *Opt. Lett.* **34**(5), 686–688 (2009).
35. Y. Avitzour, Y. A. Urzhumov, and G. Shvets, "Wide-angle infrared absorber based on a negative-index plasmonic metamaterial," *Phys. Rev. B* **79**(4), 045131 (2009).
36. E. E. Narimanov and A. V. Kildishev, "Optical black hole: broadband omnidirectional light absorber," *Appl. Phys. Lett.* **95**(4), 041106 (2009).
37. X. Liu, T. Starr, A. F. Starr, and W. J. Padilla, "Infrared spatial and frequency selective metamaterial with near-unity absorbance," *Phys. Rev. Lett.* **104**(20), 207403 (2010).
38. D. Chanda, K. Shigeta, T. Truong, E. Lui, A. Mihi, M. Schulmerich, P. V. Braun, R. Bhargava, and J. A. Rogers, "Coupling of plasmonic and optical cavity modes in quasi-three-dimensional plasmonic crystals," *Nat. Commun.* **2**, 479 (2011).
39. K. Aydin, V. E. Ferry, R. M. Briggs, and H. A. Atwater, "Broadband polarization-independent resonant light absorption using ultrathin plasmonic super absorbers," *Nat. Commun.* **2**, 517 (2011).
40. D. M. Callahan, J. N. Munday, and H. A. Atwater, "Solar cell light trapping beyond the ray optic limit," *Nano Lett.* **12**(1), 214–218 (2012).
41. W. D. Li, F. Ding, J. Hu, and S. Y. Chou, "Three-dimensional cavity nanoantenna coupled plasmonic nanodots for ultrahigh and uniform surface-enhanced Raman scattering over large area," *Opt. Express* **19**(5), 3925–3936 (2011).
42. S. Y. Chou, Unpublished (2010).
43. S. Y. Chou, P. R. Krauss, and P. J. Renstrom, "Imprint of sub-25 nm vias and trenches in polymers," *Appl. Phys. Lett.* **67**(21), 3114–3116 (1995).
44. W. Wu, B. Cui, X. Y. Sun, W. Zhang, L. Zhuang, L. S. Kong, and S. Y. Chou, "Large area high density quantized magnetic disks fabricated using nanoimprint lithography," *J. Vac. Sci. Technol. B* **16**(6), 3825–3829 (1998).
45. G. Li, V. Shrotriya, J. S. Huang, Y. Yao, T. Moriarty, K. Emery, and Y. Yang, "High-efficiency solution processable polymer photovoltaic cells by self-organization of polymer blends," *Nat. Mater.* **4**(11), 864–868 (2005).
46. W. L. Ma, C. Y. Yang, X. Gong, K. Lee, and A. J. Heeger, "Thermally stable, efficient polymer solar cells with nanoscale control of the interpenetrating network morphology," *Adv. Funct. Mater.* **15**(10), 1617–1622 (2005).
47. Z. N. Yu, H. Gao, W. Wu, H. X. Ge, and S. Y. Chou, "Fabrication of large area subwavelength antireflection structures on Si using trilayer resist nanoimprint lithography and liftoff," *J. Vac. Sci. Technol. B* **21**(6), 2874–2877 (2003).
48. P. Lalanne and G. M. Morris, "Antireflection behavior of silicon subwavelength periodic structures for visible light," *Nanotechnology* **8**(2), 53–56 (1997).
49. T. W. Ebbesen, H. J. Lezec, H. F. Ghaemi, T. Thio, and P. A. Wolff, "Extraordinary optical transmission through sub-wavelength hole arrays," *Nature* **391**(6668), 667–669 (1998).
50. W. D. Li, J. Hu, and S. Y. Chou, "Extraordinary light transmission through opaque thin metal film with subwavelength holes blocked by metal disks," *Opt. Express* **19**(21), 21098–21108 (2011).

1. Introduction

Many approaches have been proposed to solve the aforementioned three issues in solar cells. Traditionally, surface roughing and antireflection surfaces are used to enhance the light coupling [1–6]; surface roughing, cavity and waveguides are used to improve the light trapping and absorption [1–7]; and nanoscale metal wires or ultra-thin metal film are used to replace the ITO transparent conducting electrode (but suffering low transparency, high sheet resistance or both) [8–11]. Recently, significant advances in nanoscale plasmonics open up new solutions to the three issues. Some of the advances have been implemented in solar cells, such as metallic micro/nanostructures (e.g. dots, disks or lines) put inside, frontside or backside of photovoltaic active materials [11–32]. But, many of the advances are either yet being recognized to be useful to solar cells or being recognized but not tested [33–37]. For example, nanostructured-metal/insulator(lossless)/metal (nMIM) plasmonic cavities with the top metal layer in the form of disk or wire arrays have been studied as perfect light absorbers and are considered being useful to solar cells but have not been implemented [36–40].

However, a close examination reveals that a solar cell is drastically different from an nMIM cavity. In an nMIM cavity, the "lossless" insulator virtually does not absorb light and all light is absorbed by the metals and becomes heat. But in a solar cell, it needs to have a nanostructured-metal/absorbing active layer/metal (nMAM) cavity, and to have light absorbed by the active layer to create electric charge carriers, not by metals to generate heat

(wasting energy). The absorbing active layer alters cavity behavior drastically. Such fundamental differences in principles and materials require significant different cavity design and operation. Separately, it is unclear how well the metallic disk/wire layer in an nMAM cavity could replace ITO film as a transparent electrode in solar cells.

In searching for efficient photoelectron cathodes inspired by 3D cavity antenna design for ultrasensitive sensors [41], we developed a new plasmonic cavity that has a ultrathin sandwich structure of metal-mesh electrode with subwavelength holes/absorbing-semiconductor/metal-sheet (MESH/A/M), and found that such cavity is extremely efficient in coupling incident light into the absorbing semiconductor rather than the metals [42]. Here we report an implementation of the MESH/A/M cavity design into a new organic solar cell with MESH replacing ITO film (termed “plasmonic cavity with subwavelength hole-array (PlacSH) solar cell”), the first experimental study and demonstration, and the observation of several unique properties of PlacSH-SC.

2. PlacSH solar cell structure and operation

A PlacSH solar cell is a ultrathin plasmonic cavity, consisting of primarily, a thin MESH as a transparent front electrode, a thin metal back electrode, and in-between a thin light absorbing photovoltaic active material layer (namely, an MESH/A/M plasmonic cavity). All features of the MESH (i.e. the pitch, hole size and hole separation) are subwavelength (i.e. less than light wavelength). For the optical property of PlacSH, the thickness of the back electrode is insignificant, as long as it is a good metallic light reflector.

The PlacSH is designed in such way that, for a given light wavelength range (i.e. bandwidth), a significant portion of incoming light is transmitted through the MESH into the cavity, and then the most of the transmitted light is trapped and absorbed by the cavity. As shown later, the experimentally demonstrated total light absorption by the PlacSH (the lumped effect of transmission, trapping and absorption) is as high as 96% (average 90%) and broad bandwidth (e.g. nearly constant from 400 nm to 900 nm). Moreover, we observed that the PlacSH also can reduce the light reflection and absorption by MESH by 2 to 6 fold compared to that when the MESH is alone; and that the sheet resistance of a 30 nm thick MESH is 2.2 ohm/sq or less—4.5 fold or more lower than a 100 nm thick ITO film. All of these have led to a significant enhancement of solar cell performances (external quantum efficiency, open-circuit voltage, short-circuit current density, fill factor and a power conversion efficiency) as discussed below. In this demonstration of PlacSH-SCs, the photovoltaic active layer is a sub-absorption length thick layer of a bulk hetero-junction of poly (3-hexylthiophene) / [6,6]-phenyl-C61-butyric acid methyl ester (P3HT/PCBM). Our current study has focused on the effects of PlacSH-SC structure parameters on solar cell performance, rather than the effects of polymer materials, compositions or processing conditions. We used all polymers as received from commercial vendors and processed them using conventional methods, except filtering with 450 nm filter size.

A PlacSH solar cells with an optimized structure has a 30 nm thick gold MESH with a hole array of 175 nm diameter and 200 nm period (as transparent electrode) on a fused silica substrate, 10 nm thick poly(3,4-ethylenedioxythiophene):polystyrene sulfonic-acid (PEDOT:PSS) layer (electron blocking layer), 85 nm P3HT/PCBM film (active layer), 5 nm thick TiO_x (hole blocking layer) and 100 nm thick Al film (back electrode) (Fig. 1(a) and 1(b)). The incident light enters the solar cell from transparent silica substrate side through the transparent MESH. Excluding the thickness of the Al electrode and the substrate, the total thickness of the device (the active layer, the transparent front contact, and charge blocking layers) is 130 nm.

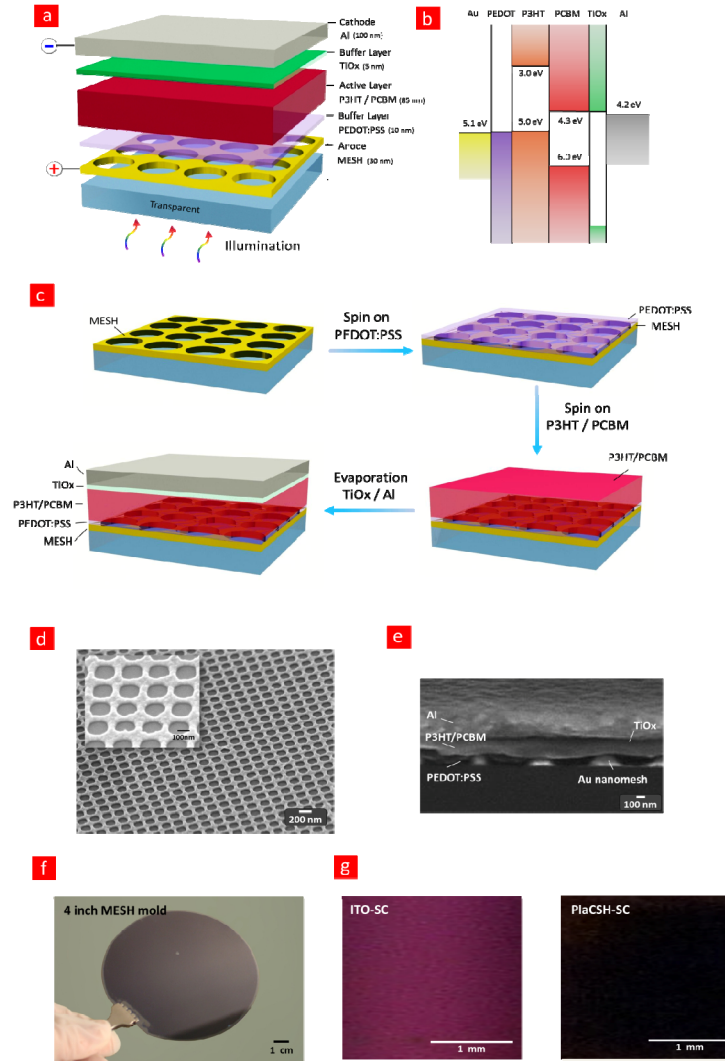


Fig. 1. Plasmonic Cavity with Subwavelength Hole-array (PlaCSH) Solar Cell (SC). (a) Schematic. PlaCSH-SC consists of an Au metallic-mesh electrode with subwavelength hole-array (MESH), a Al backplane electrode, and in between a sandwich of P3HT/PCBM, TiOx, and PEDOT:PSS layers. (b) Energy band diagram. (c) Schematic of PlaCSH-SC fabrication: fabrication of MESH by nanoimprint on a fused silica substrate, spinning of PEDOT:PSS buffer layer and P3HT/PCBM active layer, and thermal deposition of TiOx buffer layer and Al electrode. (d) Tilt-view scanning electron micrograph (SEM) of Au MESH with 175 nm diameter and 200 nm pitch hole array. (e) Cross-sectional SEM of PlaCSH solar cell. (f) Optical image of 4-inch diameter nanoimprint mold used. (g) Optical image under Sun light of PlaCSH-SC (completely black) and reference ITO-SC (dark magenta).

3. Fabrication

PlaCSH solar cells were fabricated on 4" fused silica substrates (index = 1.5). First, MESH was fabricated by nanoimprint lithography [43] using a 4" mold with sub-wavelength pitch and diameter holes over entire mold area (Fig. 1(f)) and deposition and lift-off of Au. The mold was a daughter mold duplicated by nanoimprint from a master mold which was fabricated by interference lithography and multiple nanoimprints [44]. Then the 4" MESH wafers were cut into 1 in. x 1 in. squares; followed by spinning, in nitrogen environment, the

PEDOT:PSS (annealed 15 min at 120 °C) and the P3HT/PCBM (5:4 ratio) in chlorobenzene (PEDOT:PSS from Sigma Aldrich, P3HT from Rieke Metals, PCBM from Nano-C), and then dried in covered glass petri dishes for 20 min. Finally the TiOx and Al film were evaporated through a shadow-mask to define the back electrode, followed by a post annealing at 150 °C for 30 min in nitrogen. A typical active area of each device, defined by the back electrode, is 3 mm by 3 mm. (The samples were exposed to air for a short time during the transfers between a glove box and evaporator.)

For comparison, also fabricated were the reference solar cells, “ITO-SCs”, which have the exact same device structure/materials/geometry as the PlaCSH-SCs except that the MESH is replaced by a 100 nm thick ITO. ITO has a plasma wavelength of ~1.2 μm, therefore in the wavelength range of current study, an ITO film does not have plasmonic behavior and the ITO-SC does not have a plasmonic cavity. The ITO was deposited on a fused silica substrate and was annealed at 450 °C for 1h, and after that the ITO-SCs were fabricated together with PlaCSH-SCs in the same batch.

Scanning electron microscopy (SEM) of fabricated MESH shows that the hole shape is close to square with round corners and smooth edges, and that the MESH is uniform over large area (Fig. 1(d)). SEM of the cross-section of PlaCSH solar cells further confirms that the fabricated devices have the correct structure as intended (Fig. 1(e)). The optical images under the Sun light show that PlaCSH-SC is black in color, while ITO-SC is dark magenta (Fig. 1(g)), which are related to the optical absorption spectrum of each device type as discussed later.

4. PlaCSH-SC's J-V and power conversion efficiency

Under 100 mW/cm² air mass 1.5 global solar irradiation (AM1.5G) from a solar simulator, the typical measured current density vs. voltage (J-V) curves of the optimized PlaCSH solar cells exhibit an open-circuit voltage (V_{oc}) of 0.62 V (The Al electrode is the ground), a short-circuit current density (J_{sc}) of 10.4 mA/cm², a fill factor (FF) of 67%, and a power conversion efficiency, PCE, (η_{eff}) of 4.4%; while typical ITO-SCs (the reference) have $V_{oc} = 0.62$ V, $J_{sc} = 7.4$ mA/cm², $FF = 63\%$, and $\eta_{eff} = 2.9\%$ (Fig. 2 and Table 1). Compared to ITO-SCs, PlaCSH-SCs have enhanced the PCE by 52%, and J_{sc} and FF by 41% and 6% respectively. Even without optimizing the polymer composition and processing conditions, the achieved PCE in PlaCSH-SCs is among the highest for the P3HT/PCBM material system, which was previously achievable only using active materials several times thicker (e.g. 200 nm or thicker) or optimized polymer compositions and treatments, or both [45, 46].

Table 1. Properties of PlaCSH Solar Cell and Reference ITO Solar Cell

	V_{oc} (V)	J_{sc} (mA/cm ²)	FF (%)	η_{eff} (%)
ITO-SC	0.62	7.4	63	2.9
PlaCSH-SC	0.62	10.4	67	4.4
Enhancement	0%	41%	6%	52%

The J-V characteristics in dark were measured and showed that the saturation current in PlaCSH-SCs is slightly smaller than the ITO-SCs (Fig. 2(b)), possibly due to better molecular orientation and crystallinity of the P3HT/PCBM layer on an ordered texture surface (e.g. MESH) than the flat surface of ITO.

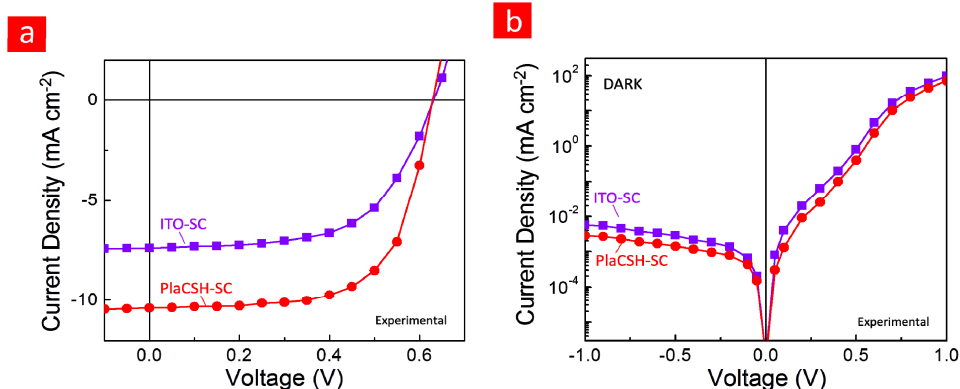


Fig. 2. Photocurrent of PlaCSH-SC and reference ITO-SC. Typical J-V characteristics measured under 100 mW/cm^2 AM 1.5 global solar irradiation (a) and in the dark (b). PlaCSH-SC has an open-circuit voltage (V_{oc}) of 0.62 V, a short-circuit current density (J_{sc}) of 10.4 mA/cm^2 , a fill factor (FF) of 67%, and a power conversion efficiency (η_{eff}) of 4.4%; while ITO-SCs have $V_{oc} = 0.62 \text{ V}$, $J_{sc} = 7.4 \text{ mA/cm}^2$, $FF = 63\%$, and $\eta_{eff} = 2.9\%$. PlaCSH-SCs have enhanced power conversion efficiency by 52%, and J_{sc} , and FF by 41% and 6% respectively.

5. PlaCSH-SC's large external quantum efficiency (EQE)

The EQE spectra of both PlaCSH-SCs and ITO-SCs were measured using a Xenon lamp (150W Oriel), a monochromator, a calibrated photodetector and collimation optics (for forming parallel normal incident light beam) (Fig. 3). The EQE of PlaCSH-SC is significantly higher than that for ITO-SC in the entire measured wavelength range (350 to 800 nm).

Specifically, the PlaCSH-SCs have a maximum EQE of 69% at 575 nm, which is 33% higher than ITO-SCs (52% at 500 nm) and red-shifted. The EQE enhancement factor (defined as the ratio of EQE of PlaCSH-SC to ITO-SC) as high as 2.2 fold (220%) at 650 nm (Fig. 3(b)).

The measured EQE spectra offer another way to estimate J_{sc} , which can be obtained by integrating the measured EQE spectrum with a standard AM 1.5G solar spectrum, leading to 10.3 and 7.4 mA/cm^2 for PlaCSH-SC and ITO-SC, respectively. This is in excellent agreement with that obtained from the direct J-V measurements, i.e. 10.4 and 7.4 mA/cm^2 . The agreement also provides a good crosscheck of our solar simulator and EQE measurements.

6. Pure-P3HT/PCBM layer's absorbance and relationship to EQE

To understand the high EQE achieved in PlaCSH, we measured (i) the absorbance spectrum of a 85 nm thick P3HT/PCBM film on a fused silica substrate (pure-P3HT/PCBM film) (Fig. 3(a)) and (ii) the transmittance spectrum of three different thickness (42 nm, 72 nm, and 92 nm) P3HT/PCBM film on glass to obtain the absorption-length spectrum (Fig. 3(b)).

Compared to the measured pure-P3HT/PCBM absorbance spectrum, the EQE spectrum of ITO-SC has an identical peak wavelength and almost the same shape in wavelength dependence, indicating that the EQE in ITO-SC is dominated by the absorption in the P3HT/PCBM layer (i.e. the photovoltaic active-layer) and there is virtually no plasmonic cavity effect, as expected. However, in contrast, the EQE spectrum of PlaCSH-SC differs significantly from the pure P3HT/PCBM absorbance spectrum in several aspects: peak wavelength (575 nm rather than 500 nm), peak value, and spectrum shape (broadband vs. narrow band). These differences are due to the plasmonic cavity effect of PlaCSH as further discussed below.

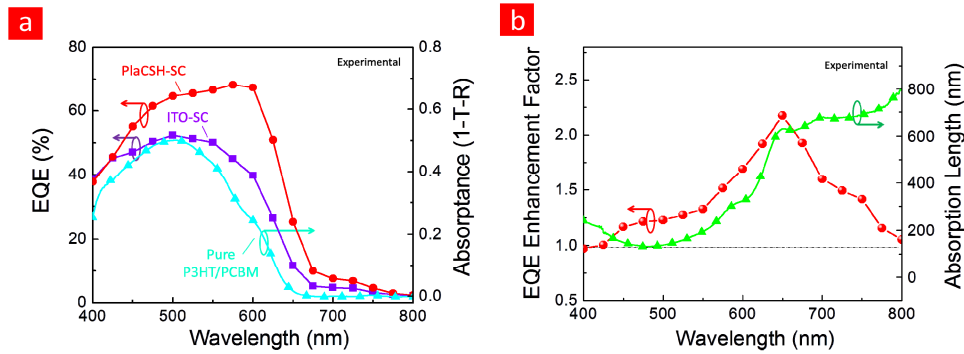


Fig. 3. EQE spectrum of PlaCSH-SC and ITO-SC and Absorption-length in P3HT/PCBM (85 nm thick on glass). Measured external quantum efficiency (EQE) spectrum of PlaCSH-SC and ITO-SC as well as the measured absorbance spectrum of 85 nm thick P3HT/PCBM film on glass (a), and EQE enhancement (EQE ratio of PlaCSH-SC to ITO-SC), and measured absorption-length in P3HT/PCBM (b). PlaCSH-SC achieved a maximum EQE of 69% at 575 nm wavelength where the 85 nm thick active layer's single pass absorbance is only 27%. And PlaCSH-SC has an EQE enhancement factor always larger than one over the entire measured spectrum range, and can be as high as 2.2 fold (220%) at 650 nm.

The absorption length spectrum in the pure-P3HT/PCBM film was measured from the light transmittance spectrum of the three different thickness is 138 nm and 267 nm at 500 and 575 nm wavelength respectively, and was found to be 250 nm when averaged over 400 to 650 nm wavelength range (Fig. 3(b)). The absorption length spectrum is consistent with the direct absorbance spectrum measurement of an 85 nm thick film on glass (Fig. 3(a)). From the measured absorption-lengths, we can calculate the single-pass absorbance in the P3HT/PCBM active layer, which is merely 27% for an 85 nm thick film at 575 nm wavelength. Yet the EQE of the PlaCSH-SC with such thin active layer is 69% at 575 nm wavelength. Such high EQE achieved in an active material of less than one third (1/3) of absorption length thick is due to a good light transmission and trapping in the PlaCSH. Without the plasmonic cavity, like ITO-SC, the EQE is much lower, as shown clearly by the measurements (Fig. 3(a)).

7. Broad-bandwidth, up-to-96% light coupling and absorbance in PlaCSH solar cell

We measured the normal incident reflectance spectra (R) (400 to 900 nm wavelength) of the PlaCSH-SCs and ITO-SCs, and then obtained the normal incident absorbance spectra (A) using $1-R-T$, where transmittance (T) is zero in the SCs (Fig. 4). We found that for the optimized PlaCSH-SCs, they have (a) a low normal incident reflectance of a minimum of 4.3% (at 750 nm wavelength) and an average of 10%, and hence a high absorbance of a maximum of 95.7% and an average of 90%; (b) a broad bandwidth for the low reflectance and high absorbance—nearly constant over the entire bandwidth measured (400-900 nm) (namely the bandwidth of the PlaCSH-SC is wider than the wavelength range of our current measurements), (c) a reflectance that can be even lower than the reflectance directly from pure P3HT/PCBM layer on glass, and (d) an absorbance spectrum is drastically different from that of a pure P3HT/PCBM layer on glass.

For ITO-SCs, on the other hand, the normal incident reflectance and absorbance are significantly worse than PlaCSH-SCs, and have a spectrum behaving drastically different from PlaCSH-SCs but similar to (hence dominated by) the P3HT/PCBM active layer absorbance, which is relatively narrow band. The ITO-SC's normal incident reflectance has a minimum of 20% (at 482 nm wavelength) and an average of 56%, giving an absorbance of a maximum of 80% and an average of 44%.

At the wavelength of 500 nm (the absorption peak for pure P3HT/PCBM layer), 575 nm (the EQE peak for PlaCSH-SC) and 790 nm (outside of the P3HT/PCBM absorption), the

absorptance in PlaCSH-SC is, respectively, 1.13, 1.4 and 18 fold (e.g. 113%, 140%, and 1,800%) higher than ITO-SC (Fig. 4(b)). The broadband high absorption and low reflection in PlaCSH-SC are due to good light coupling and trapping in PlaCSH.

Since the incident light enters from the fused silica substrate, the interface between air and the substrate has a normal incident reflectance of 4%. Subtracting this reflection, the normal incident reflectance of PlaCSH-SC is as low as 0.3%.

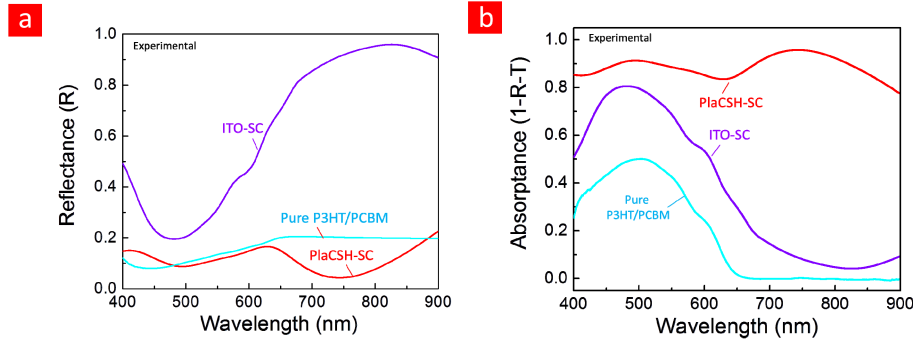


Fig. 4. Normal Incident Reflectance and Absorptance spectra of PlaCSH-SC, ITO-SC, and P3HT/PCBM (85 nm thick on glass). Measured normal incident optical reflectance spectrum (a) and measured absorptance spectrum (1-reflectance-transmittance). PlaCSH-SC has a normal incident reflectance as low as 5% and 10% average and absorptance as high as 96% and 90% average over a broad band (400 to 900 nm). ITO-SC has normal incident reflectance of minimum 20% and 56% average, and absorptance 80% maximum and 44% average. At 650 and 790 nm wavelength, the absorptance in PlaCSH is 2.9 and 18 fold higher than ITO-SC. The shape of absorptance spectrum in ITO-SC is dominated by that of P3HT/PCBM layer, but not in PlaCSH-SC.

8. Electrical and optical properties of MESH-only on glass

To better understand PlaCSH, we measured the properties of each of its components. Beside the active layer (discussed above), we measured the sheet-resistance as well as the spectra of reflectance, transmittance and hence absorptance of (a) 30 nm thick Au MESH's with 200 nm hole pitch and different hole diameters (175, 125, and 75 nm) on glass (i.e. fused silica) without any other components of PlaCSH (MESH-only), and (b) the annealed 100 nm thickness ITO on glass (ITO-only) which is identical to that used in ITO-SC (Fig. 5 and Table 2). In the optical measurements, the incident light enters from the glass substrates to have identical situation as the solar cells.

The sheet-resistance measurements with 'four probes method' (Fig. 5(a)) show that (a) the 100 nm thick annealed ITO film has 10 ohm/sq sheet-resistance, among the best reported, indicating a good ITO quality; (b) the MESH's have sheet-resistances much smaller than the ITO film: even the worst sheet-resistance (175 nm diameter holes) is still 2.2 ohm/sq—4.5 fold (450%) better than ITO; and (c) the smaller the hole diameter is, the smaller sheet resistance of MESH, but a higher light reflectance and absorptance. A smaller sheet resistance can improve fill-factor and power conversion efficiency, hence is highly desirable.

The reflectance measurements show (a) for the 200 nm pitch, the larger the hole diameter of MESH is, the smaller the light reflectance; and (b) for 175 nm diameter holes the MESH-only's reflectance can be smaller than the ITO-only in wavelength of 470 to 700 nm (Fig. 5(b)).

The transmittance/absorptance measurements show (a) the absorptance of ITO-only is ~10% and nearly constant over the entire measured wavelength range; and (b) almost all MESH-only's measured have an absorptance higher than ITO-only, except the MESH-only with 175 nm diameter holes and at the wavelengths longer than 640 nm (Fig. 5(c), 5(d)).

Table 2. Electrical and Optical Properties of MESH-only and ITO-only

Electrode type	Peak Transmittance (%)	Sheet Resistance (Ω/\square)
100 nm thick ITO	90	10
70 nm dia. hole MESH	26	0.7
125 nm dia. hole MESH	42	1.0
175 nm dia. hole MESH	81	2.2

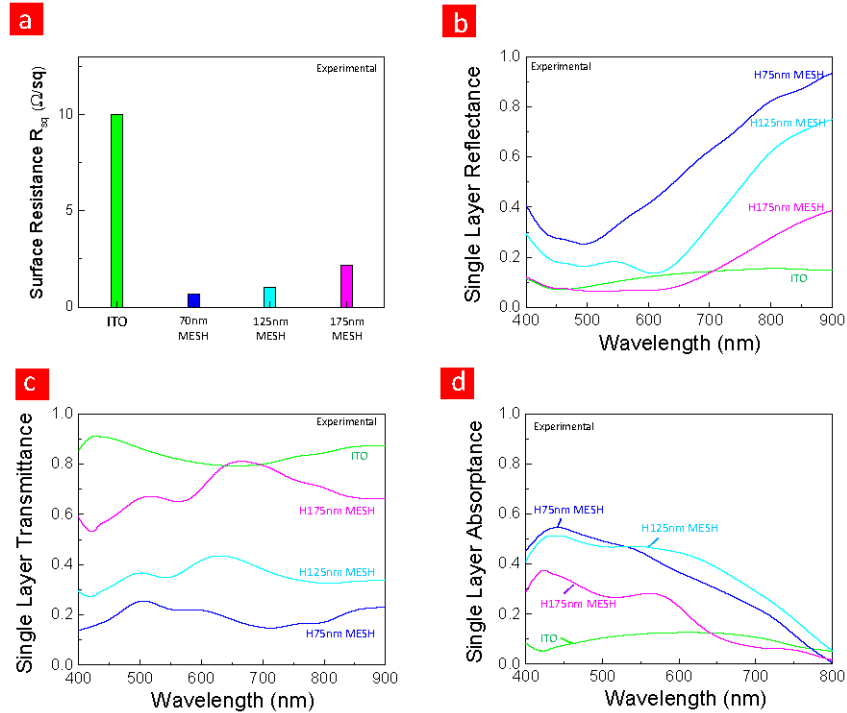


Fig. 5. Optical and electrical properties of metallic electrode with subwavelength hole-array (MESH). Measurements of sheet-resistance (a), reflectance (b), transmittance (c), and absorbance (d) of 30nm thick Au MESHs on glass (MESH-only) with 75nm, 125nm and 175 nm hole size and 200 nm period as well as the 100 nm thick annealed ITO film on glass (ITO-only). The measured sheet-resistance is 10 ohm/sq for of the ITO, but 2.2 ohm/sq or less for the MESH's –making them at least 4.5 fold better. The smaller the hole diameter is, the smaller the sheet resistance of MESH, but higher light reflectance and absorbance. Compared with Fig. 4, after PlaCSH-SC formation, both the reflectance and absorbance of MESH drop significantly by 2 to 5 fold in reflectance and as large as 6.7 fold in absorbance at 500nm wavelength. In contrast, for the ITO, the reflectance, after ITO-SC formation, increases drastically by 2 to 5.8 fold.

9. Comparison of MESH optical property before and after PlaCSH-SC formation

Interestingly, we found that after forming the PlaCSH-SC, both the reflectance and absorbance of the MESH drop significantly (Comparison of Fig. 4 and 5). The measurements show that at wavelength of 700, 750 and 800 nm, the reflectance for MESH-only is, respectively, 14%, 20% and 28%, but it drops to 7%, 4% and 8% after the PlaCSH formation, leading to reflectance reduction ranging from 2 to 5 fold. In contrast, for ITO-SC, the reflectance has increased drastically: from 9% and 14% for ITO-only to 20% and 85% after SC formation at the wavelength of 500 and 700 nm, respectively, leading to a reflectance increase of 2 to 5.8 fold. The increase in the reflectance after ITO-SC formation is due to the additional reflections at the interface of P3HT/PCBM layer and the Al contact; while the

decrease in reflectance after PlaCSH-SC formation is due to the plasmonic cavity effects that lead to excellent light coupling and trapping in the active layer of PlaCSH-SC.

The reduction of light absorption in MESH after PlaCSH formation can be seen by analyzing the measured EQE, reflectance and absorptance in PlaCSH-SC and ITO-SC. For ITO-SC measured at 500 nm wavelength, it has 20% reflectance, 52% EQE, and 10% ITO layer absorptance, leading to 18% of total incident energy (i.e. 26% of the energy after passing ITO film) becoming heat in the active layer and Al back electrode. For PlaCSH-SC measured at 500 nm wavelength, the reflectance is 9% and the EQE is 64.5%, hence the total energy absorbed in the active layer and Al electrode is 87%, if assuming PlaCSH-SC has the same ratio of electrical energy to heat energy in the active layer and Al electrode as ITO-SC. Thus, at 500 nm wavelength the absorptance in the MESH after PlaCSH formation is 4%, which is 6.7 fold smaller than 27% absorptance in the MESH-Only, and 2.5 fold smaller than 10% absorptance in the ITO-only film.

Our simulation shows that the reduction in light absorption in MESH after PlaCSH formation is attributed better light coupling and focusing into the active polymer layer when PlaCSH is formed (to be published elsewhere).

Moreover, compared to previous nanoscale metal wires used to replace the ITO transparent conducting electrode [8–11], the MESH's reported here have much smaller sheet resistance, lower reflectance and higher transmittance. Our simulations show that they are attributed to the properties related to the plasmonic cavity effects of PlaCSH as well as the subwavelength sizes in all features (i.e. the pitch, hole size, and hole separation) of MESH (to be reported elsewhere). It should be noted that the previous approaches use subwavelength width wires but longer than wavelength separation, which causes many no-zero order diffractions and hence reduces the light transmission.

10. Broad-band, Omni acceptance

We measured the effects of incident light angle (0° to 75° with a 15° increment) and polarization on the photocurrent and reflectance of the PlaCSH-SCs and ITO-SCs (Fig. 6). (Note: The maximum incident angle can be measured is limited by the current SC device size). The photocurrents were measured using a polarized broad-band white light (halogen lamp) and is plotted in the relative change to the photocurrent of PlaCSH-SC for normal incident light (i.e. 0°) (Fig. 6(a)). The results clearly show that the PlaCSH-SC has much smaller dependence on angle and polarization than ITO-SC. For examples, at incident angle of 45° , 60° and 75° , the measured photocurrent change for PlaCSH-SC is only 1.8%, 10% and 22%, respectively, for s-wave, and 1.6%, 0.2% and 11% for p-wave; while the photocurrent change for ITO-SC is 11%, 34% and 85% for s-wave, and 1.4%, 7% and 43% for p-wave. This means that at angle $\geq 45^\circ$, the reflectance of PlaCSH-SC is 3 to 6 fold smaller (hence better) than ITO-SC for s-wave and 4 to 7 fold smaller for p-wave.

The measured angle and polarization dependence of the photocurrent of the PlaCSH-SC and ITO-SC is consistent with that of their reflectance (Fig. 6(b)). We measured the angle dependence on reflection using a polarized white light for the wavelength range from 350 to 850 nm (Fig. 6(c)). Compared to ITO-SC, the light reflection (hence coupling into solar cell) in PlaCSH-SC is nearly independent of light polarization and incident angle over entire angle range measured. We term this property "Omni acceptance". The high, broad-band, Omni light acceptance in PlaCSH-SC has made it look black under the Sun light (Fig. 1(g)), and is over 2 fold better than Si subwavelength antireflection (either roughed surfaces or periodic nanostructures) [47, 48] at high angles, yet PlaCSH has a thickness over 10 fold thinner.

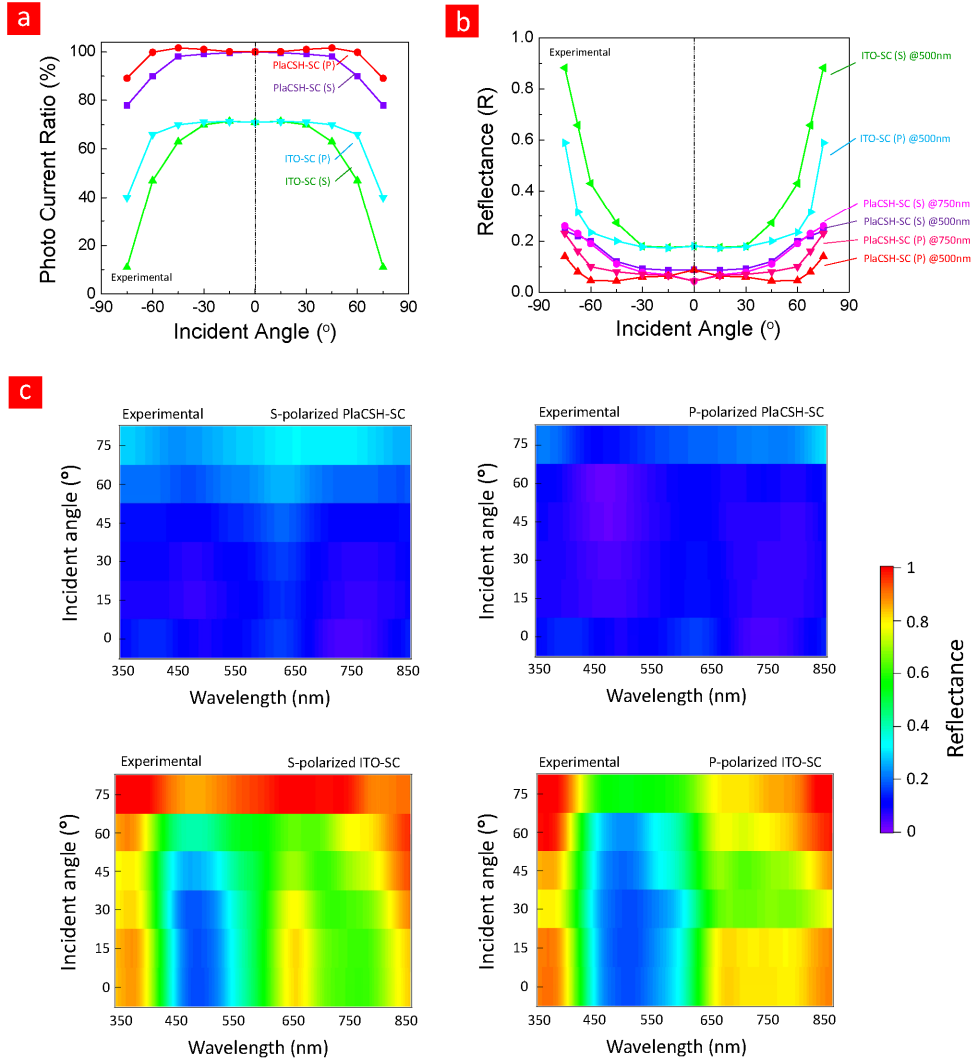


Fig. 6. Broad-band Omni acceptance (near angle and polarization independence) in PlaCSH-SC. Measured incident light angle and polarization dependence of photocurrent under a white light (a), reflectance at 500 nm and 750 nm wavelength (b), and reflectance spectra under a white light (c) for PlaCSH-SC and ITO-SC (The photocurrent is scaled to that of PlaCSH at normal light incident). They show that the angle and polarization dependence of photocurrent under white light in PlaCSH is significantly less than ITO-SC by a factor of 3 to 6 fold for s-wave and 4 to 7 fold for p-wave. The photocurrent changes observed are consistent with the measured reflectance changes. The property of PlaSCH-SC, that light coupling into solar cell is nearly independent of light polarization and incident angle over entire possible angle, is termed “Omni acceptance”. The achieved high, board-band, Omni light acceptance of PlaCSH is 2 to 3 fold better than that of Si subwavelength antireflection, yet PlaCSH has a thickness over 10 fold thinner.

Furthermore, we measured the incident angle and polarization dependence of light reflectance and transmittance of the substrate only (i.e. a fused silica). Our analysis of the data indicates that the angle and polarization dependence of reflectance for PlaCSH-SCs can be even smaller, if the light enters the solar cell without going through the glass substrate, which can be achieved by building the MESH front electrode on the top of PlaCSH-SC (Details will be published elsewhere).

11. Comparison with MIM cavity

To further study PlaCSH, we fabricated the structures same as the PlaCSH-SC and ITO-SC except replacing the photovoltaic active layer by a non-light absorbing insulator—a PMMA (polymethylmethacrylate) layer of 110 nm thick (the same optical thickness as 85 nm P3HT/PCBM); and measured their optical spectra (R, T, and A) in the wavelength range of 400 to 900 nm (Fig. 7). We also doubled-checked experimentally that indeed the PMMA is an insulator and has little light absorption in the measured wavelength range. Thus the nMAM cavity becomes an nMIM cavity, while ITO/A/M structure become ITO/I/M.

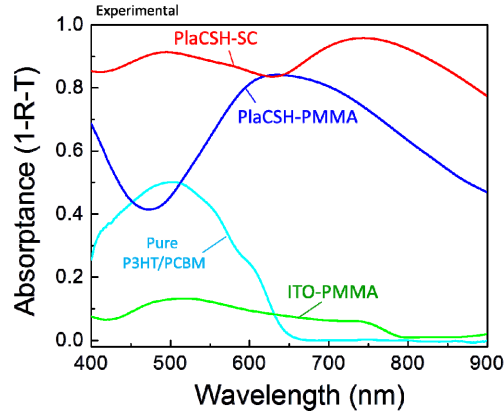


Fig. 7. Measured absorbance spectrum of MIM and Comparison with MAM. The measured absorbance spectrum of PlaCSH-SC (MESH/Absorbing active layer/Metal) and the structures same as PlaCSH-SC and ITO-SC except replacing the absorbing active layer (P3HT/PCBM) by PMMA of the same optical thickness (MESH/Insulating (lossless)/Metal). They show the absorbing layer changes the optical property of a plasmonic cavity significantly. Using of an absorbing layer changes a plasmonic cavity from narrow band to broadband, and increases the absorption substantially.

A comparison of the measured spectra shows (a) the ITO/PMMA/Al structure has a very small absorbance and a nearly flat spectrum, which are almost identical to the absorbance of ITO film. This indicates that PMMA indeed does not absorb much light in wavelength range tested, and that again the absorbance spectrum of ITO-SC is dominated by the active material (P3HT/PCBM). And (b) the PlaCSH with PMMA (an nMIM cavity) has an absorbance spectrum drastically different from (i) the ITO/PMMA/Al (no active layer nor plasmonic cavity), (ii) the PlaCSH-SC (an nMAM cavity), and (iii) the pure P3HT/PCBM film in the following ways. (1) Compared to the ITO/PMMA/Al, the absorbance of the nMIM (PlaCSH with PMMA) is 9.4 times larger on average. The absorption enhancement is caused by better light coupling and trapping in the nMIM's plasmonic cavity. (2) Compared to the PlaCSH-SC, the nMIM has a smaller absorbance (except at 540 nm where they are equal) and a narrower bandwidth. And (3) compared to the pure P3HT/PCBM film, the nMIM has an absorption peak nearly twice large, a different peak position (650 nm vs. 550 nm), and a slightly wider bandwidth.

These comparisons indicate that an nMIM and an nMAM are drastically different plasmonic cavities; the replacing of the non-light-absorbing insulator in an nMIM cavity with a light-absorbing material can significantly improve both the total cavity absorption and absorption bandwidth.

12. Effects of cavity length of PlaCSH

Clearly the cavity length of PlaCSH also plays an important role in PlaCSH-SC performance. The cavity length of the PlaCSH includes the active layer thickness plus certain light

penetration depth into the front and back electrode layers. By fabricating and testing PlaCSH-SCs with different P3HT/PCBM active layer thickness of 50, 82, 100 and 130 nm, we found that the highest photocurrent, the highest PCE and a favorable absorption spectrum are achieved with 85 nm P3HT/PCBM thickness, while a thinner or thicker thickness gives a worse photocurrent, PCE and absorption spectrum (Fig. 8). We attribute these effects primarily to the plasmonic cavity, where an optimized design can lead to (i) a better light coupling into the P3HT/PCBM active layer in a PlaCSH and (ii) an optimum interplay between light trapping and energy loss to heat inside the plasmonic-cavity, although the effect of cavity length on the charge carrier diffusion and collection in the polymer might also play a role.

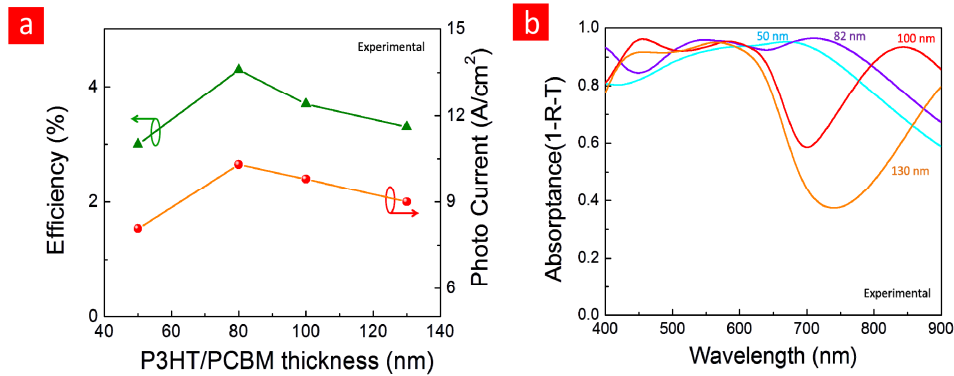


Fig. 8. Cavity length effect on efficiency, photocurrent, and absorbance of PlaCSH-SC. Power conversion efficiency (a) and absorbance spectrum (b) for PlaCSH-SC with different P3HT/PCBM layer thickness of 50, 82, 100, and 130 nm, showing that the ~85 nm thickness gives the best performance.

13. Physics and optimization of PlaCSH-SC

The unique properties observed in the PlaCSH-SC (e.g. greatly enhancing the light coupling, trapping, and absorption in a sub-absorption-length active layer, while reducing the light reflectance and absorbance in MESH) are due to the special properties of the nM/A/M plasmonic cavity of PlaCSH.

In a classic Fabry-Perot cavity, a good light trapping inside the cavity requires a high reflectivity on both end mirrors, which means that only tiny portion of the incident light can enter the cavity and the rest of them are reflected back and hence wasted—bad for a solar cell. However, unlike a Fabry-Perot cavity, the PlaCSH has (1) the MESH as the front surface of the plasmonic cavity, where the properties of the metal (plasmonic), the open holes, and the subwavelength sizes of the holes and the separation will make a significant portion of incident light transmit through the MESH to inside the cavity with a small reflection; and (2) the back metal layer (plane) placed near and parallel to the MESH will further enhance the light transmission through the MESH from outside to inside the cavity and then trap light there. (As shown in our experiments: 95.7% light transmission and trapping).

The light transmission through the MESH is not hard to understand, since the MESH has subwavelength size open holes in the metal thin film, which is known for having extraordinary light transmission [49] (Note: Previous work do not have subwavelength hole separation and hence have a light transmission significantly less than the MESH). What less obvious or what most interesting is why the back metal layer (plane) placed nearby the MESH can enhance the transmission and the trapping of the light? A simple explanation is as follows. Just the MESH alone, there are evanescent waves (so-called surface plasmon polaritons) on both surfaces of the thin metal film, which determine the light transmission and reflection. When another metal structure (e.g. the back metal layer or other metal structures)

is placed in a vicinity of the holes of the MESH, the evanescent waves will be coupled with the new metal, greatly enhancing the transmission of the light into the new metal side. Such phenomenon has been observed by us previously in extraordinary light transmission through “blocked” holes [50]. When the new metal is an optical opaque metal sheet such as the back metal layer used in PlaCSH, the light passed through the MESH will be completely reflected back by the metal sheet, and will be localized around each hole inside the cavity in the form of local plasmons, hence trapping the light there. More details of the theory and simulation will be presented elsewhere.

From the physical picture above, it is clear that the properties of the PlaCSH depend on the properties of (i) the MESH (metal optical property, geometry of the holes and separation, and film thickness), (ii) the active layer (optical properties and thickness), (iii) the cavity length and (iv) the back metal layer (metal optical property). The current work has optimized only some of the key parameters.

14. Broad-band Omni-acceptance effects on scattering light harvesting

The broad-band Omni acceptance of PlaCSH-SC demonstrated here has a significant impact to practical power conversion efficiency (PCE) in harvesting scattered light, which is dominant in cloudy days and in the morning and evening (Note: The effect of Omni acceptance to PCE is relatively small under the direct Sun light, where the light receiving is dominated by the light projection onto a flat solar-cell). We calculated the upper-limit of the additional PCE enhancement of a flat PlaCSH-SC over a flat ITO-SC due to Omni acceptance in detecting s-polarized and unpolarized scattered light for different material index (Fig. 9), which is 81% (s-wave, leading to a total 175% increase, namely 8% PCE) and 41% (unpolarized) for the PlaCSH-SC using P3HT/PCBM (index of 2.2), and 142% and 61% for silicon PlaCSH-SC (index of 3.5).

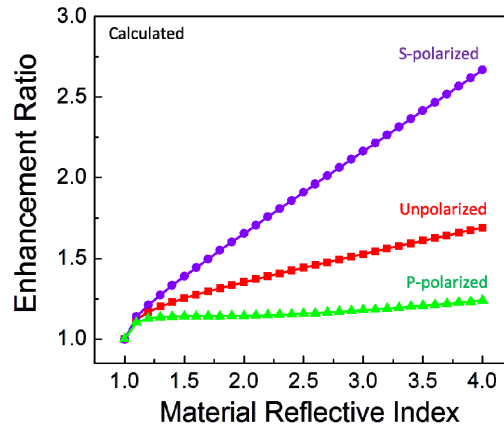


Fig. 9. Calculated upper-limit of additional enhancement in conversion efficiency of PlaCSH over ITO solar cells due to Omni acceptance for detecting s and p-wave and unpolarized scattered light as a function of material index. For s-polarized light and unpolarized light, the additional enhancement of PlaCSH-SC in power conversion efficiency over ITO-SC due to Omni acceptance (enhancement factor upper-limit) is 81% and 41%, respectively, for the PlaCSH-SC using P3HT/PCBM (index of 2.2); and 142% and 61% for silicon PlaCSH-SC (index of 3.5).

15. Summary

We proposed, studied and demonstrated a new ultra-thin high-efficiency organic solar cell, “plasmonic cavity with subwavelength hole-array solar cell (PlaCSH-SC)”, that has a high light coupling, trapping and absorption in a sub-absorption-length-thick active layer, and replaces the indium-tin-oxide (ITO) transparent electrode with MESH. Experimentally, the

PlaCSH-SCs with 85 nm thick organic active layer and 30 nm thick Au MESH of 175 nm diameter holes (200 nm pitch) have achieved a light coupling-efficiency/absorptance as high as 96%, average 90%, broad-band, and Omni acceptance; and an external quantum efficiency of 69% for 27% single-pass active layer absorptance (at 575nm wavelength); leading to a power conversion efficiency (PCE) under standard solar irradiation of 4.4% that is 52% higher than the reference ITO-SC. The PCE is also among the highest for the P3HT/PCBM material system previously achievable only using active material several times thicker or optimized polymer compositions and treatments, or both. In detecting scattered light, the Omni acceptance can significantly increase the organic PlaCSH-SC's PCE by additional 81% over ITO-SC, leading to a total 175% increase (8% PCE). Furthermore, we found that the light reflection and absorption by MESH after formation of PlaCSH are reduced significantly from the values by 2 to 6 fold when it is alone, and that a typical MESH has sheet resistance of 2.2 ohm/sq or less—over 4.5 fold lower than the best value reported in 100 nm thick ITO film, giving a lowest reflectance-sheet-resistance product, plus low absorption and high transmission. Fabrication of PlaCSH used nanoimprint on 4" wafer and is scalable to roll-to-roll manufacturing. The performance of organic PlaCSH-SC can be significantly improved by further optimization. The designs, fabrications, and findings are applicable to thin solar cells in other materials (organic or inorganic) and on thin substrates such as plastic films.

Supplement materials

Solar cell J-V measurements and solar simulator

The J-V characteristics of the solar cells were measured using HP 4145B semiconductor analyzer. The solar simulator for 100 mW/cm² AM 1.5 global solar irradiation consists of a Xenon lamp (150W Oriel) and an AM 1.5 G optical filter (Newport Corporation, Air Mass Filter, 81094) with the total power density at 100 mW/cm², which was set by using a broadband radiation power-meter (Newport, Radiant Power Meter and Probe, 70260 Radiant Power Meter with 70268 Probe). The solar simulator was calibrated in two independent methods. (1) We measured the irradiation intensity spectrum of the solar simulator, compared it with the published solar spectrum, and found that they agree. And (2) we tested our solar cells using a different solar simulator in another research Lab and achieved an identical J-V as using our own solar simulator.

Measurements of reflection and transmission spectra

The reflectance and transmittance spectra were measured with a white (wide-band) light source using halogen bulb guided by a fiber (Euromex Fiber Optic Light Source), beam collimation optics, a spectrometer (Horiba Jobin Yvon), and light collection and detection system (a 10 × microscope objective (Numerical Aperture N.A = 0.25), an optical fiber, and then photodetector). The collimation optics consist of a 10x microscope objective and a pin hole that expand the light from a fiber into a parallel beam, and a second pin hole near the sample to further shape the light beam size and parallel ness. For angle-dependent and polarization reflectance measurements, two rotation stages were used: one for the sample and another for collecting the reflected light.

Calculation of additional power conversion efficiency (PCE) enhancement due to Omni acceptance in scattering light harvesting

The upper-limit of the additional PCE enhancement of PlaCSH-SC in scatted light harvesting is defined as the ratio of the total absorption of ideal PlaCSH-SC (A_{PLH}) to that of traditional-SC (A_c):

$$Ratio(n, p) = \frac{A_{PLH}}{A_c} = \frac{\int (1 - R_{PLS}) I(\theta, p) d\Omega}{\int (1 - R_c(n, \theta, p)) I(\theta, p) d\Omega} \quad (1)$$

where on R_{PLS} and R_c is the reflectance of PlaCSH-SC and conventional SC respectively, $I(\theta, p)$ is the scattered light intensity (which is assumed to be a constant in simplified model), the angle Ω integration is over 2π solid angle, n is the material index, p is a given polarization. For the upper limit, we assume the PlaCSH-SC has an ideal Omni acceptance of scattering light, which is fully independent of angle and polarization ($R_p = 0$). For conventional SC, the reflectance is assumed to be from a planar surface between the air and the material of the index n , and obey the Fresnel equations for the dependence on the material index, angle and polarization (R_c).

Contributions

S.Y.C. originated the idea of PlaCSH and PlaCSH solar cells, designed and directed the research. W.D. and S.Y.C. designed, fabricated and characterized the devices. And S.Y.C. and W.D. analyzed data and wrote the manuscript.

Acknowledgment

We thank Yuxuan Wang and Dr. Weihua Zhang for discussions in preparing the manuscript, Dr. Liangcheng Zhou and Weihua Zhang for assistance in optical setups, other members of NanoStructure Laboratory at Princeton University for their supports, and Defense Advanced Research Projects Agency (DARPA), Office of Naval Research (ONR), and National Science Foundation (NSF) for partially funding the work.